Journal of
Ship&Ocean
Technology
©JUNE 2002

SOTECH Vol. 6, No. 2, pp. 12~22, 2002

Numerical and Experimental Studies of Dual Subsea Pipelines in Trench

Chul H. Jo[1], Young S. Shin[2] and Kyoung H. Min[1]

[1]Department of Naval Architecture and Ocean Engineering Inha University; E-mail: chjo@inha.ac.kr
[2]Department of Mechanical Engineering Halla University

Abstract

Offshore pipelines play an important role in the transportation of gas, oil, water and oil products. It is common to have a group of pipelines in the oil and gas field. To reduce the installation cost and time, dual pipelines are designed. There are great advantages in the installation of dual pipelines over two separate single lines. It can greatly reduce the cost for trench, back-filling and installation. However the installation of dual pipelines often requires technical challenges. Pipelines should be placed to be stable against external loadings during installation and design life period. Dual pipelines in trench can reduce the influence of external forces. To investigate the flow patterns and forces as trench depth and slope changes, number of experiments are conducted with PIV(Particle Image Velocimetry) equipment in a Circulating Water Channel. Numerical approaches to simulate experimental conditions are also made to compare with experimental results. The velocity fields around dual pipelines in trench are investigated and analysed. Comparison of both results show similar patterns of flow around pipelines. It is proved that the trench depth contributes significantly on hydrodynamic stability. The trench slope also affects the pipeline stability. The results can be applied in the stability design of dual pipelines in trench section. The complex flow patterns can be effectively linked in the understanding of fluid motions around multi-circular bodies in trench.

Keywords: dual pipeline, trench, PIV, drag reduction, spectral method

1 Introduction

In the development and operation of subsea satellite oil wells, more than one pipes are required along the route. For multiple pipe arrangements, it is difficult to determine the flow patterns around them and their effects by surrounding pipeline on the stability(Rados and Pitt 2000). To ensure a continuous operation of the system, adequate design criteria and considerations are required(Knoll and Herbich 1980, Garrison 1980).

External loads to subsea pipeline resting on ocean bottom are a function of parameters associated with waves and currents acting around the pipeline. There have been numbers of studies conducted to develop a criteria to predict hydrodynamic loads imposed by external waves and currents. But not much for dual pipelines in trench section. Quite number of dual pipelines in many

regions are required to be trenched for protection from anchoring or fishing activities. However clear guidelines are not available to confirm the stability in trench. Also the clear guidelines for the reduction of hydrodynamic loads of pipelines in trench are not provided except very limited arrangements and conditions.

In this research the relationship between the trench depth and hydrodynamic force at various slopes and flow velocity is investigated experimently and numerically. A numerical study is conducted with Navier-Stokes and the continuity equations. Since trench geometries with dual pipes are very complex, grid shapes distributed near the intersection between pipes and trench are considered very important to obtain stable solutions. The elliptic transformation method is applied to get a smoothly distributed and clustered grid. The generalized spectral method which is applicable to more general partial differential equations and boundary conditions is used to solve the pressure equation satisfying the continuity equation. It is well known that the oscillating lift and drag forces occur in the uniform flow around a circular body. Understanding this phenomenon, time advancements are proceeded until obtaining harmonically steady state. Number of physical models are installed and experimented at three current speeds with various trench section slopes and depths in a circulating water channel. The flow patterns around dual cylinder models in trench are measured by the PIV system. Reduction coefficients for drag over various experimental cases are obtained. The reduction coefficients proposed in the paper for various cases at different slopes and depths can be applied to understand the stability of dual pipelines in trench sections.

2 Theory

2.1 Numerical modeling

The non-dimensional equations for the conservation of mass and momentum for an incompressible viscous fluid can be written as

$$D \equiv \frac{\partial u}{\partial x} + \frac{\partial v}{\partial y} = 0 \tag{1}$$

$$\frac{\partial u}{\partial t} + u\frac{\partial u}{\partial x} + v\frac{\partial u}{\partial y} = -\frac{\partial p}{\partial x} + \frac{1}{R}(\frac{\partial^2 u}{\partial x^2} + \frac{\partial^2 u}{\partial y^2}) \tag{2}$$

$$\frac{\partial v}{\partial t} + u\frac{\partial v}{\partial x} + v\frac{\partial v}{\partial y} = -\frac{\partial p}{\partial y} + \frac{1}{R}(\frac{\partial^2 v}{\partial x^2} + \frac{\partial^2 v}{\partial y^2}) \tag{3}$$

Here, all variables are non-dimensionalized by the effective velocity on sea bottom u_e and the pipe diameter D, and R is Reynolds number. A time advancement scheme for (2) and (3) can be written as

$$\frac{u^{n+1}}{\Delta t} = \frac{u^n}{\Delta t} + F^n - \frac{\partial p^n}{\partial x} \tag{4}$$

$$\frac{v^{n+1}}{\Delta t} = \frac{v^n}{\Delta t} + G^n - \frac{\partial p^n}{\partial y} \tag{5}$$

where F and G are defined as

$$F \equiv \frac{1}{R}(\frac{\partial^2 u}{\partial x^2} + \frac{\partial^2 u}{\partial y^2}) - u\frac{\partial u}{\partial x} - v\frac{\partial u}{\partial y} \tag{6}$$

$$G \equiv \frac{1}{R}(\frac{\partial^2 v}{\partial x^2} + \frac{\partial^2 v}{\partial y^2}) - u\frac{\partial v}{\partial x} - v\frac{\partial v}{\partial y} \tag{7}$$

By substituting (6) and (7) into (1), the pressure equation may be derived as

$$\nabla^2 p^n = R^n \tag{8}$$

where

$$R^n = \frac{D^n}{\Delta t} + {F_x}^n + {G_y}^n \tag{9}$$

The pressure (8) may be expressed in the generalized coordinate form as follows:

$$\alpha p_{\xi\xi} - 2\beta p_{\xi\eta} + \gamma p_{\eta\eta} + \delta_p p_\xi + \delta_q p_\eta = \frac{D}{\Delta t} + \xi_x F_\xi + \eta_x F_\eta + \xi_y G_\xi + \eta_y G_\eta \tag{10}$$

where

$$\begin{aligned} \alpha &= \nabla\xi \cdot \nabla\xi \\ \beta &= -\nabla\xi \cdot \nabla\eta \\ \gamma &= \nabla\eta \cdot \nabla\eta \\ \delta_p &= \nabla^2\xi \\ \delta_q &= \nabla^2\eta \end{aligned} \tag{11}$$

and superscript n is omitted in convenience. Equation (10) is solved to obtain the velocity field at the n+1 time level.

2.2 Numerical analysis

The spectral method was used to solve (10). Equation (10) may be rearranged as

$$\begin{aligned} &\alpha_0 p_{\xi\xi} - 2\beta_0 p_{\xi\eta} + \gamma_0 p_{\eta\eta} + \delta_{p0} p_\xi + \delta_{q0} p_\eta \\ &= R - (\alpha - \alpha_0)p_{\xi\xi} - (-2\beta + 2\beta_0)p_{\xi\eta} - (\gamma - \gamma_0)p_{\eta\eta} - (\delta_p - \delta_{p0})p_\xi - (\delta_q - \delta_{q0})p_\eta \end{aligned} \tag{12}$$

where α_0, ... , δ_{q0} are mean coefficients of α, ... , δ_q in the ξ direction respectively. The pressure may be expanded in Fourier series in the ξ direction as follows:

$$p_{\xi\xi} = p_k(\eta)e^{ik\xi} \tag{13}$$

Then $p_\xi$and p can be obtained by integrating (13) as follows:

$$p_\xi = \frac{p_k(\eta)}{ik}e^{ik\xi} + p_0(\eta)\xi + a(\eta) \tag{14}$$

$$p = \frac{p_k(\eta)}{(ik)^2}e^{ik\xi} + \frac{1}{2}p_0(\eta)\xi^2 + a(\eta)\xi + b(\eta) \tag{15}$$

By substituting (13), (14) and (15) into (12), the ordinary differential equation may be derived as

$$\begin{aligned}&\left[\frac{\gamma_0(\eta)}{(ik)^2}\ddot{p_k}(\eta)+\left\{\frac{-2\beta_0(\eta)}{ik}+\frac{\delta_{q0}(\eta)}{(ik)^2}\right\}\dot{p_k}(\eta)+\left\{\alpha_0(\eta)+\frac{\delta_{p0}(\eta)}{ik}\right\}p_k(\eta)\right]e^{ik\xi}\\&+\frac{\gamma_0}{2}(\eta)\xi^2\ddot{p_0}(\eta)+\left\{-2\beta_0(\eta)\xi+\frac{\delta_{q0}(\eta)}{2}\xi^2\right\}\dot{p_0}(\eta)+\delta_{p0}(\eta)\xi p_0(\eta)+\gamma_0(\eta)\xi\ddot{a}(\eta)\\&+\{-2\beta_0(\eta)+\delta_{q0}\eta\xi\}\dot{a}(\eta)+\delta_{p0}(\eta)a(\eta)+\gamma_0(\eta)\ddot{b}(\eta)+\delta_{q0}(\eta)\dot{b}(\eta)=\overline{R}(\xi,\eta)\end{aligned}\tag{16}$$

where

$$\begin{aligned}\overline{R}=R&-(\alpha-\alpha_0)p_{\xi\xi}-(-2\beta+2\beta_0)p_{\xi\eta}\\&-(\gamma-\gamma_0)p_{\eta\eta}-(\delta_p-\delta_{p0})p_\xi-(\delta_q-\delta_{q0})p_\eta\end{aligned}\tag{17}$$

Equation (16) may be written in each spectral mode as follows:

$$\frac{\gamma_0(\eta)}{(ik)^2}\ddot{p_k}(\eta)+\left\{\frac{-2\beta_0(\eta)}{ik}+\frac{\delta_{q0}(\eta)}{(ik)^2}\right\}\dot{p_k}(\eta)+\left\{\alpha_0(\eta)+\frac{\delta_{p0}(\eta)}{ik}\right\}p_k(\eta)=\overline{M_k}(\eta),\quad k=1,2....\tag{18}$$

$$\gamma_0(\eta)\ddot{b}(\eta)+\delta_{q0}(\eta)\dot{b}(\eta)=\overline{M_0}(\eta)\tag{19}$$

where $\overline{M_k}(\eta)$ is the m^{th} spectral mode of $\overline{M}(\xi,\eta)$ and

$$\begin{aligned}\overline{M}(\xi,\eta)=&\overline{R}(\xi,\eta)\\&-\frac{\gamma_0}{2}(\eta)\xi^2\ddot{p_0}(\eta)-\left\{-2\beta_0(\eta)\xi+\frac{\delta_{q0}(\eta)}{2}\xi^2\right\}\dot{p_0}(\eta)-\{\alpha_0(\eta)+\delta_{p0}(\eta)\xi\}p_0(\eta)\\&-\gamma_0(\eta)\xi\ddot{a}(\eta)-\{-2\beta_0(\eta)-\delta_{q0}(\eta)\xi\}\dot{a}(\eta)-\delta_{p0}(\eta)a(\eta)\end{aligned}\tag{20}$$

From the boundary condition at the ξ ends, $p_0(\eta)$ and $a(\eta)$ may be obtained as

$$p_0(\eta)=\frac{\dot{p}(\xi_1,\eta)-\dot{p}(\xi_2,\eta)}{\xi_1-\xi_2}\tag{21}$$

$$a(\eta)=\frac{p(\xi_1,\eta)-p(\xi_2,\eta)}{\xi_1-\xi_2}-\frac{\xi_1+\xi_2}{2}p_0(\eta)\tag{22}$$

Equation (12) are solved iteratively to obtain convergent pressure fields.

2.3 Applied theory

Pipelines in open trench is subjected to external loads such as wave and current(Sumer 1997). The schematic diagram of Figure 1 shows the drag forces acting around dual pipes in open trench.

The drag force in trench can be estimated with reduction coefficients which vary with trench depth(H) and slope. The relating equations are as described below(Jo et al 2000):

$$F^*{}_{Dn}=F_D\times RF_{Dn}\tag{23}$$

where

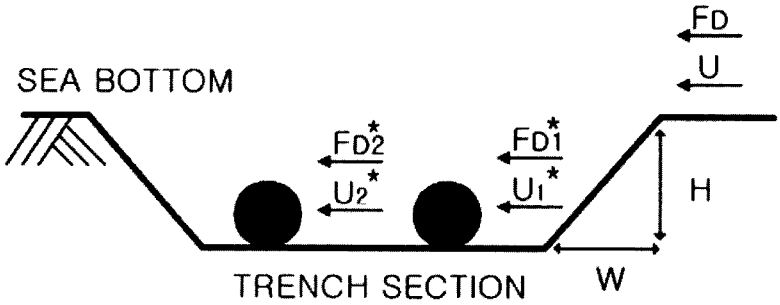

Figure 1: Dual pipelines in open trench

F^*_{Dn} : drag force per unit length in open trench on individual pipeline
RF_{Dn} : reduction coefficient on drag force on individual pipeline
F_D : drag force per unit length on sea bottom

The reduction coefficients are dependent on velocity reduction factor and Reynolds number. The velocity reduction factor can be obtained from the measurement of velocity both on seabed and in trench. The velocity reduction factor can be derived from (24):

$$\beta_n = \frac{u^*_{en}}{u_e} \tag{24}$$

where

β_n : reduction factor on velocity for individual pipeline
u_e : effective velocity of flow on sea bottom
u^*_{en} : effective velocity of flow in open trench for individual pipeline

As per the velocity reduction factor, the drag forces and reduction coefficients in trench can be written as follows:

$$RF_{Dn} = \frac{F^*_{Dn}}{F_D} = \frac{C^*_{Dn}}{C_D}\beta_n{}^2 \tag{25}$$

where

C^*_{Dn} : coefficient of drag force in open trench for individual pipeline
F^*_{Dn} : drag force per unit length on individual pipeline
RF_{Dn} : reduction coefficient on drag force for individual pipeline
F_D : drag force per unit length on sea bottom
C_D : coefficient of drag force on sea bottom

3 Numerical and experimental modeling

3.1 Numerical modeling

A grid is generated by application of the elliptic transformation(Steger and Sorenson 1979). Figure 2 shows the generated grid around the dual pipes in trench. The uniform flow is used as the initial condition. No slip condition is used at the trench bottom and pipes. The periodic boundary

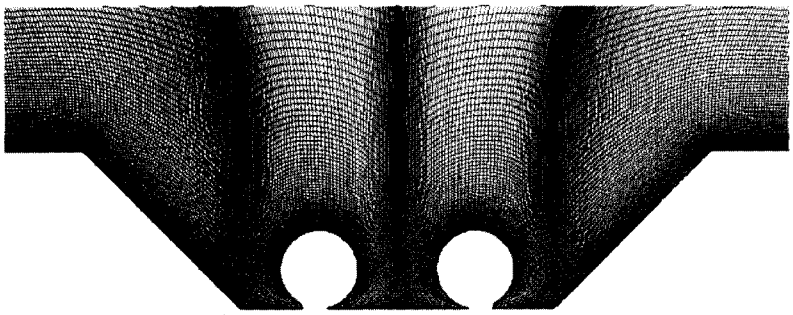

Figure 2: Schematic diagram of grid generation

conditions are applied at inflow and downstream boundaries. Time increments are taken sufficiently small to satisfy C.F.L. condition.

3.2 Experimental modeling

Figure 3 represents a schematic diagram of experimental arrangement of dual pipes in a trench. In the figure, D and H stand for outside diameter and trench depth, respectively. The space of dual pipes is fixed at D. The pipes are placed from the end of trench at the distance of $D/2$. The frames for the trench section are made out of bronze, and the seabed of transparent flexi-glass of $5mm$ thickness. The experiments are conducted in a circulating water tunnel at various current speeds as shown in Figure 4. The test section of the water tunnel is $3.5m$ long, and has a cross section of $1.2m$(width) and $0.9m$(height) and water depth of $0.7m$.

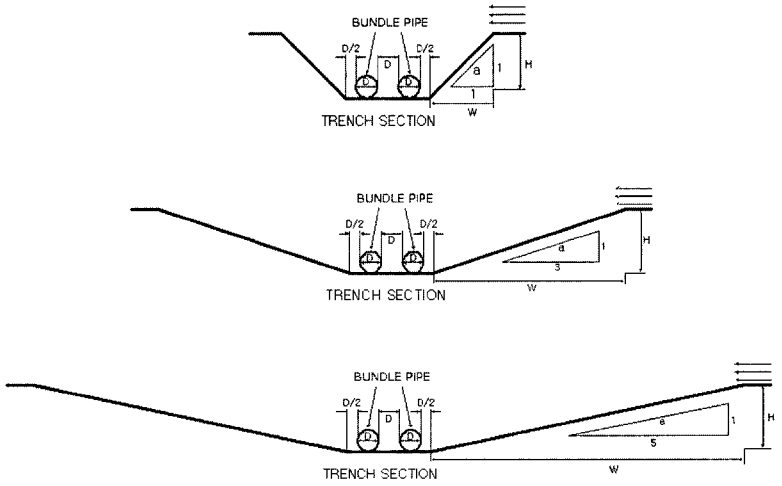

Figure 3: Schematic diagram of dual pipes in trench

To minimize side-wall effects, the models are installed $15cm$ apart from the wall having the width to diameter ratio to be about 30. Placing the measuring plane at the center of the model the side-wall effect is minimized. The models are also set up above $30cm$ from the tank bottom

and securely fastened by two support piles downstream, and free of any vibration effect. The steel support at upstream behind and below the model prevents any turbulence effect in the trench.

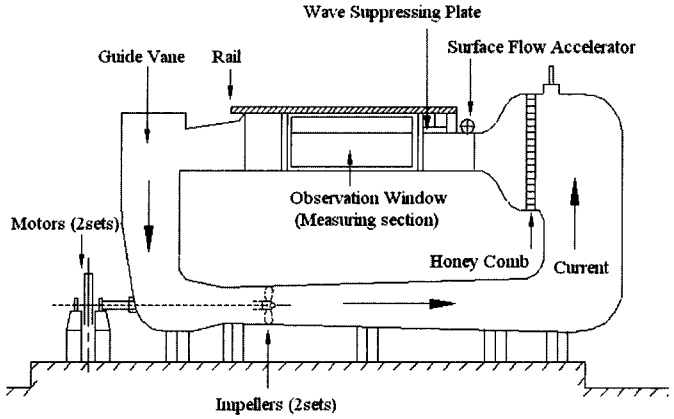

Figure 4: Schematic diagram of water tunnel

3.3 P.I.V. measurements

To identify velocity fields in the trench with various slopes, the P.I.V. measurements are performed with an optical setup illustrated in Figure 5. To provide the trench with two-dimensional sheet of light in the symmetric plane, a $1.0W$ Ar-ion laser is supplied to the flow field through a fiber optic cable together with a cylindrical lens. The particles of 150-200μm diameter having about same density with water are seeded in the tunnel after static electricity is suppressed. The visual images are captured by a CCD(Charge Coupled Device) camera(SONY-XC77RR) and stored on a tape via a video recorder. The captured images controlled by AOM are sent to odd and even fields and processed in an image board(DT3155, 640480 pixels) of a host computer.

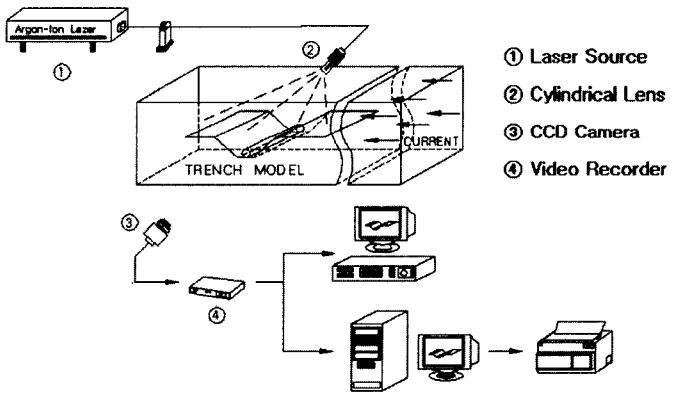

Figure 5: Experimental setup for P.I.V. measurement

4 Result and discussion

The velocity fields around the circular bodies in various trench sections are obtained numerically and experimentally. From these, velocity reduction factors and drag reduction coefficients are investigated as the reduction factors are represented as the ratio between seabed and trench section. Should it be 0.5, it means that the drag force on a body is the half over that on the seabed. As cylindrical pipes are placed in a trench, both the drag and the lift forces are reduced considerably depending on the position of the pipes in trench. This is due to the sheltering effect by the trench. It was reported that even in the same trench depth a steeper slope results in a higher reduction effect in terms of pipeline stability.

The parameters of geometrical importance may be listed as the slope length(W), trench depth(H), cylinder diameter(D). Two non-dimensional parameters are determined by H/D, and W/H. To investigate the current effect on the drag force, the case of $0.2m/s$, $0.3m/s$ and $0.4m/s$ are selected. The models having H/D of 2, 4, and W/H=1, 3 are selected. The identical conditions are also applied in the numerical approach to compare with the experimental results.

4.1 Mean flow pattern in open trench

The computed and measured velocity vectors around dual pipes in various trench configurations are compared. For the case of H/D=2 and W/H=1 with current velocity $0.2m/s$, the flow fields are presented in Figure 6. The separated shear-layer in the fore part of the trench produces several vortex motions.

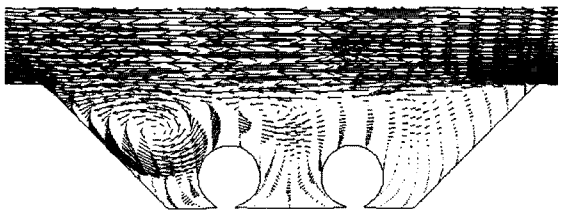

(a) Computed(W/H=1, H/D=2)

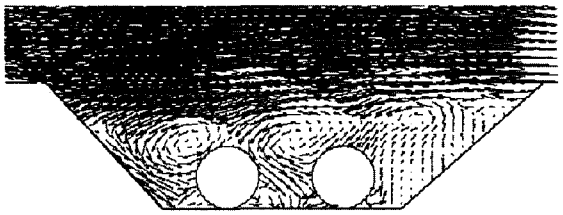

(b) Measured(W/H=1, H/D=2)

Figure 6: Compared mean-velocity patterns(current velocity is $0.2m/s$)

4.2 Drag coefficient for various depths

Figure 7 shows drad reduction factors for various cover depths. Comparing two different trench depths, H/D=2, H/D=4, when H/D is 2 there are not much difference in the drag reduction factor between upstream pipe and downstream of pipe. However when H/D becomes 4 the drag reduction factor of downstream pipe are larger than upstream. There is same tendency in computed and measured results. They indicate that the effects of trench depth is not so much significant in the stability of dual pipes. Contrary to general expectation, it shows that as the trench depth increases the reduction factor of downstream pipe increases.

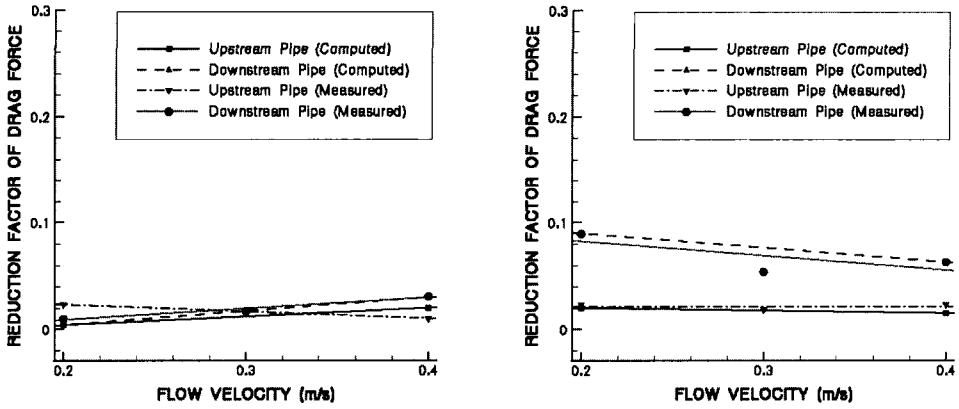

(a) H/D=2 (b) H/D=4

Figure 7: Drag force reduction factor vs. cover depth (W/H=1)

4.3 Drag coefficient for various slopes

The drag reduction coefficients for various trench slopes are as shown in Figure 8. Figures indicate that as the slope increases the reduction factor decrease. The results show that the reduction factors and coefficients for slope W/H=3 is much larger than those for slope W/H=1. When W/H=1, there are not much of differences in the drag reduction factor between upstream and downstream of pipes. But the drag reduction factor of upstream pipe is much larger than downstream one when W/H=3. This trends are revealed very similar between measured and computed results. However, it seems that the slope influences more significantly to the reduction factors than the trench depth.

4.4 Drag coefficient for upstream and downstream

The drag reduction factors for upstream and downstream around dual pipes are shown in Figures 9. They indicate that the drag reduction factor of upstream pipe are smaller than downstream when W/H=1. On the contrary, the drag reduction factor of upstream pipe is larger than downstream

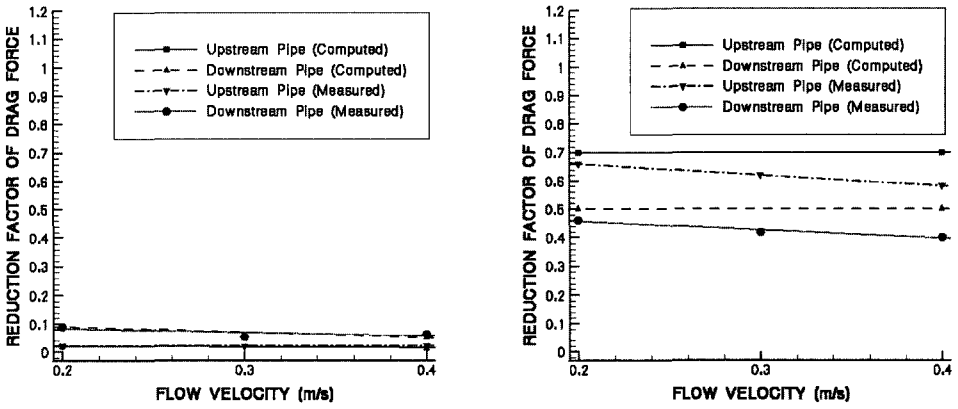

(a) W/H=1 (b) W/H=3

Figure 8: Drag force reduction factor vs. trench slope(H/D=2)

when W/H=3 for computed and measured results. They show similar tendency in the both results for various flow velocities.

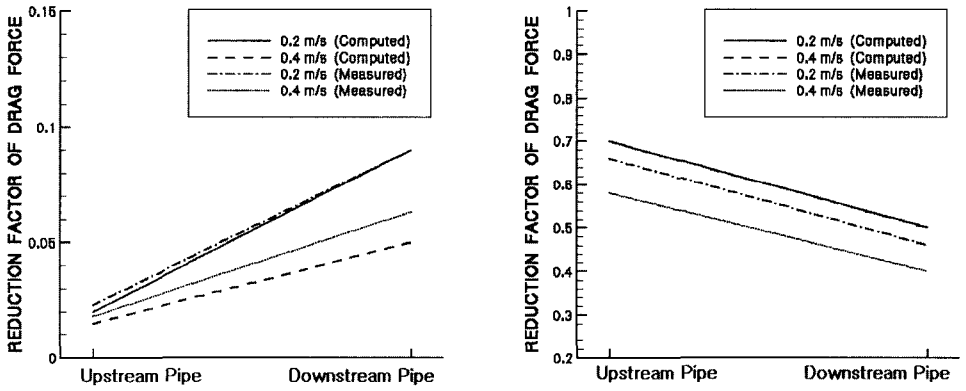

(a) W/H=1 (b) W/H=3

Figure 9: Drag force reduction factor for upstream and downstream(H/D=4)

5 Conclusion

The flow patterns around dual pipelines in trench and the drag reduction factors are investigated for various trench configurations. From numerical and experimental studies, it is observed that the effects of trench depth is not very significant in the stability of dual pipes spaced at D in trench. On the contrary, the deeper trench depth may induce an increase of drag force on the downstream of pipe as the current speed increases. The trench slope greatly influence on reduction factors. The slope W/H=1 shows significant effect in reducing the reduction factor. As the trench slope increases reduction factors remarkably becomes smaller. The drag force acting on the downstream of pipe is not always smaller than the upstream. For example, a larger drag force is noticed on the downstream of pipe when W/H=1. This study can contribute in the understanding of complex flow patterns around multi-cylindrical bodies and the reduction of drag force for various trench configurations.

References

GARRISON, C.J. 1980 A review of drag and inertia forces on circular cylinders. Offshore Technology Conference, pp. 205-218

JO, C.H., KIM, K.S. AND HONG, S.G. 2000 Subsea Pipeline in Various Trench Sections. International Offshore and Polar Engineering Conference, **2**, pp. 218-225

KNOLL, D.A. AND HERBICH, J.B. 1980 SWave and current forces on a submerged offshore pipeline. IOffshore Technology Conference, pp. 227-234

RADOS, K.G. AND PITT, D. 2000 On the Interaction of Pipe Lines on the Seabed. International Offshore and Polar Engineering Conference, **2**, pp. 155-161

STEGER, J.L. AND SORENSON, R.L. 1979 Automatic mesh-point clustering near a boundary in grid generation with elliptic partial differential equations. Journal of computational physics **33**, pp. 405-410

SUMER, B.M. 1997 Hydrodynamics around circular structures. World Scientific